



# [X/Fe] Marks the Spot: Mapping Chemical Azimuthal Variations in the Galactic Disk with APOGEE

ZOE HACKSHAW <sup>1</sup>, KEITH HAWKINS <sup>1</sup>, CARRIE FILION <sup>2</sup>, DANNY HORTA <sup>3</sup>, CHERVIN F. P. LAPORTE <sup>4</sup>,  
CHRISTOPHER CARR <sup>5</sup> AND ADRIAN M. PRICE-WHELAN <sup>3</sup>

<sup>1</sup>*Department of Astronomy, The University of Texas at Austin, 2515 Speedway Boulevard Austin, TX 78712, USA*

<sup>2</sup>*Department of Physics & Astronomy, The Johns Hopkins University, Baltimore, MD 21218, USA*

<sup>3</sup>*Center for Computational Astrophysics, Flatiron Institute, 162 5th Ave., New York, NY 10010, USA*

<sup>4</sup>*Institut de Ciències del Cosmos (ICCUB), Universitat de Barcelona (IEEC-UB), Martí i Franquès 1, E-08028 Barcelona, Spain*

<sup>5</sup>*Department of Astronomy, Columbia University, 550 West 120th Street, New York, NY 10027, USA*

6-14

arxiv:2405.18120v1

Reporter: Baokun Sun

# Outline

- 1. Introduction
- 2. Data
- 3. Methods
- 4. Results and Discussion
- 5. Summary

# Introduction

- We can use the Milky Way and its resolved Galactic components as a laboratory to answer questions about Galactic evolution and characterize the hierarchical formation (Davis et al. 1985) of the Milky Way.
- One of the most prominent trends in the Milky Way is the existence of the negative **radial and vertical metallicity gradients**.
- These gradients could provide supporting evidence for certain formation theories of the Milky Way, such as the **‘inside-out’** formation theory (Larson 1976).
- **Chemical azimuthal substructure** in the Milky Way has been previously identified using a variety of different tracers such as Hii regions and Cepheids.

- The initial sample of stars from the Gaia data release (DR17, Abdurro'uf et al. 2017b).
- We place an error cut on the effective temperature ( $T_{\text{eff}}$ ) from the Gaia catalog, selecting stars with  $3500 < T_{\text{eff}} < 5000 \text{ K}$  as well as a cut on the metallicity ( $[Fe/H]$ ), selecting stars with  $[Fe/H] > -1.0$ .
- We removed any stars with  $[O/H] > 0.5$  or  $[Mg/H] > 0.5$  to ensure a clean sample of thin disk stars.
- We required all thin disk stars to have a parallax  $\rho > 80\%$ , which was provided by the Gaia pipeline.

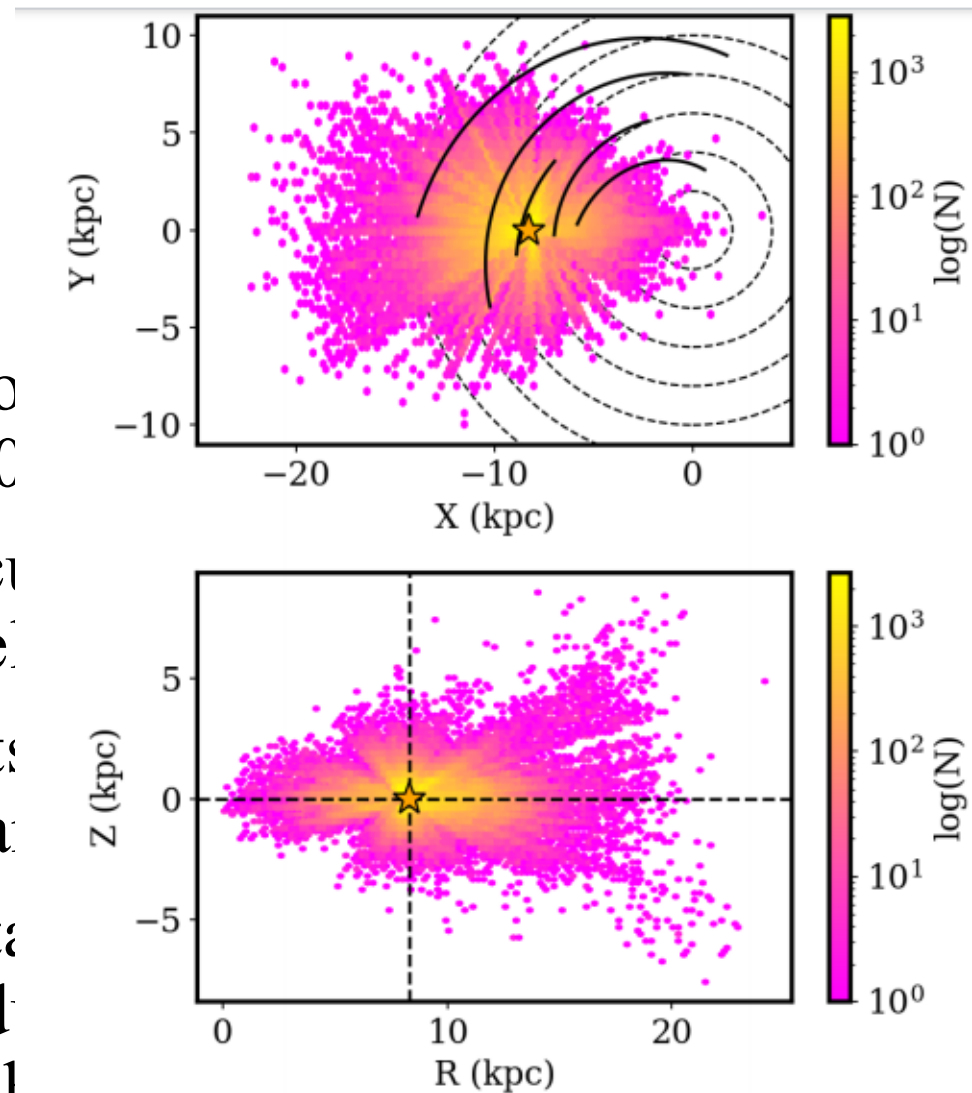


**Figure 1.** The face-on (top) and edge-on (bottom) distribution of our thin disk sample of 202,510 stars in which the hexagonal bins are colored by the logarithmic number of stars. The black contours in the top panel are the spiral arms of the Milky Way determined by Reid et al. (2019). The orange star in both panels represents the Sun.

data release (DR17, al. 2017b).

obtained from the

range  $3500 < T_{\text{eff}} <$

$5000 \text{ K}$  as well as a cut on  $[Fe/H]$ ,  $[Fe/H] > -1.0$ , which is the most relevant in our

sample. The parallax  $\rho > 80\%$ , which was provided by the Gaia pipeline, is shown in Figure 1.

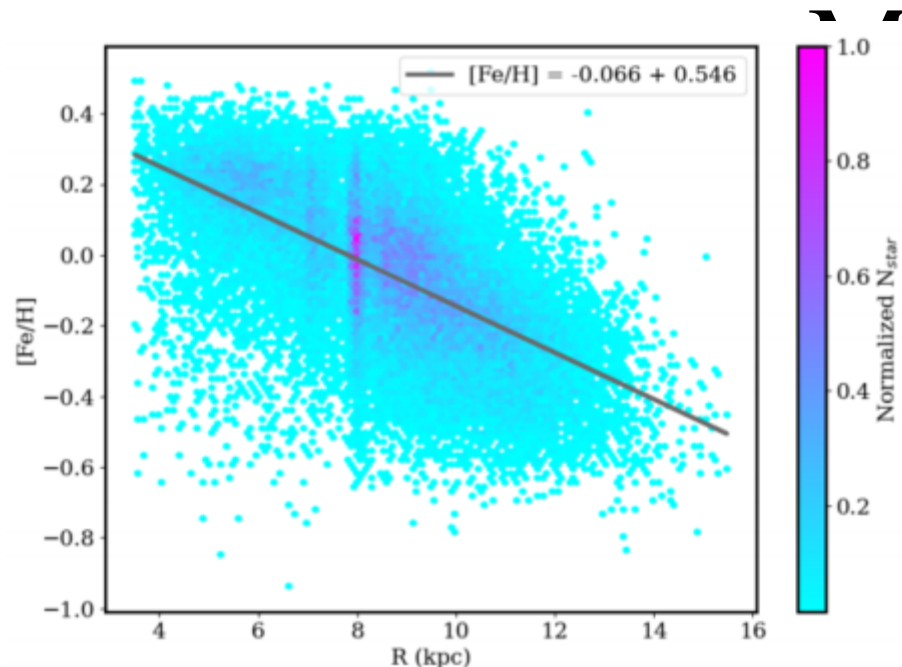


**Figure 2.** The  $[\text{Fe}/\text{H}]$  abundances with respect to Galactocentric radius of our planar thin disk sample. The artifact at  $R \sim 8$  kpc is an observational effect of the over-representation of stars in the solar neighborhood. We fit a linear model to the colored data points (column-normalized planar thin disk sample) which is represented by the grey line. From this, we obtain a metallicity gradient of  $\Delta[\text{Fe}/\text{H}]/\Delta R -0.066 \pm 0.0004$  dex/kpc and a y-intercept of 0.546 dex for the stars in our planar thin disk sample.

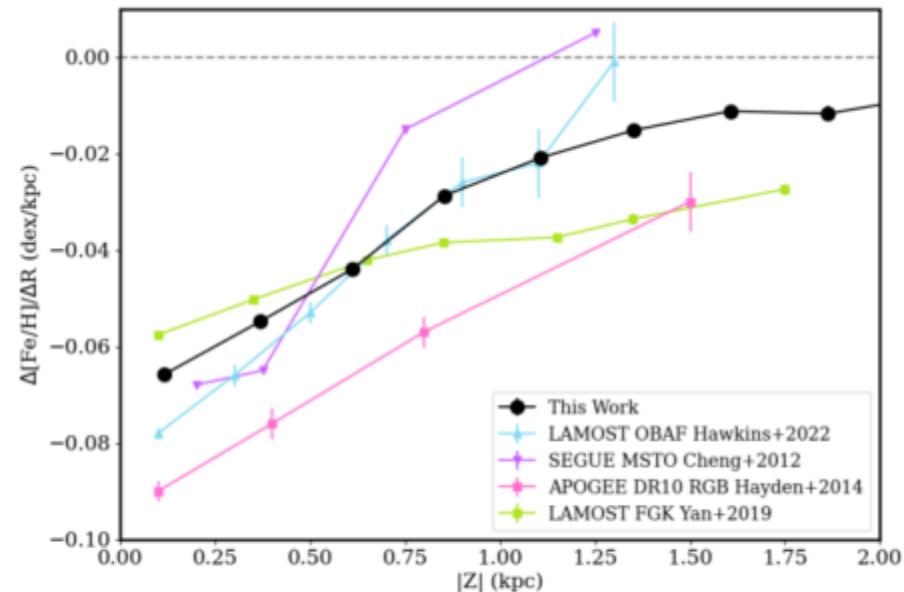


**Figure 3.** The radial metallicity gradient as a function of absolute vertical height  $Z$  above (and below) the plane. The gradient derived in this work is represented by the black dots, compared to a variety of other studies that use different tracers [Cheng et al. (2012) (purple triangles), Hawkins (2022) (blue triangles), Hayden et al. (2014) (pink squares), Yan et al. (2019) (green squares)]. Consistently,  $\Delta[\text{Fe}/\text{H}]/\Delta R$  starts off at its most negative in the plane and shallows out with greater distances from the disk. A vertical line is plotted at  $\Delta[\text{Fe}/\text{H}]/\Delta R=0$  to illustrate where the radial gradient is no longer negative. The points derived in this work lie generally in the middle of the other studies conducted.



# Metallicity Gradients

- We find that the vertical metallicity gradient is heavily correlated with Galactocentric radius in that  $\Delta[\text{Fe}/\text{H}]/\Delta Z$  approaches zero with increasing distance from the Galactic center.

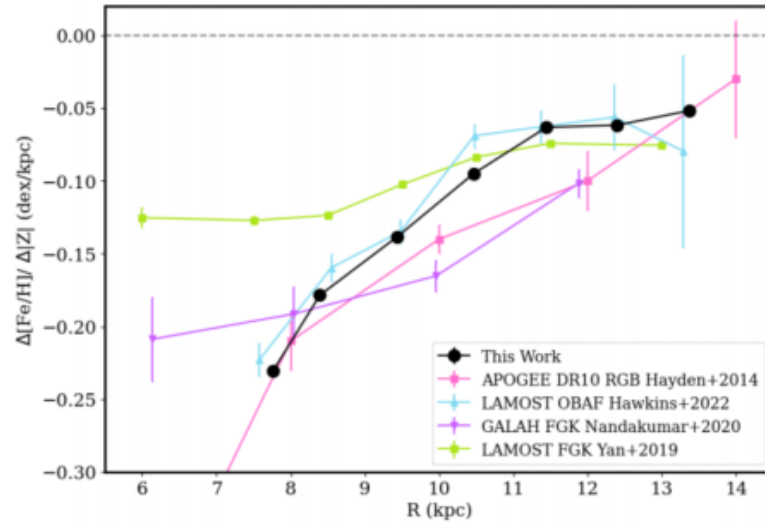


**Figure 4.** The vertical metallicity gradient as a function of Galactocentric radius. The gradient derived in this work is depicted by black dots, whereas the other colored points represent the gradient as determined by different tracers in other studies [Hayden et al. (2014) (pink squares), Hawkins (2022) (blue triangles), Nandakumar et al. (2020) (purple triangles), Yan et al. (2019) (green squares)]. The vertical metallicity gradient is at its most negative closest to the Galactic center and shallows out ( $\Delta[\text{Fe}/\text{H}]/\Delta Z$  approaches 0) as distance increases.

**Table 2.** Vertical Metallicity Gradient Parameters for R bins in the full thin disk sample

$ R $ (kpc)	$\Delta[\text{Fe}/\text{H}]/\Delta Z$ (dex/kpc)	$\sigma\Delta[\text{Fe}/\text{H}]/\Delta Z$ (dex/kpc)	$N_{\text{stars}}$
7.5	-0.2307	0.0026	29634
8.5	-0.1785	0.0022	49208
9.5	-0.1383	0.0025	33837
10.5	-0.0951	0.0026	22099
11.5	-0.0632	0.0028	14729
12.5	-0.0617	0.0030	8025
13.4	-0.0518	0.0034	3090

# Azimuthal Variations in $\Delta[\text{Fe}/\text{H}]/\Delta R$

- We follow the steps outlined in Section 3 and compute the model linear  $\Delta[\text{Fe}/\text{H}]/\Delta R$  gradient throughout the disk.

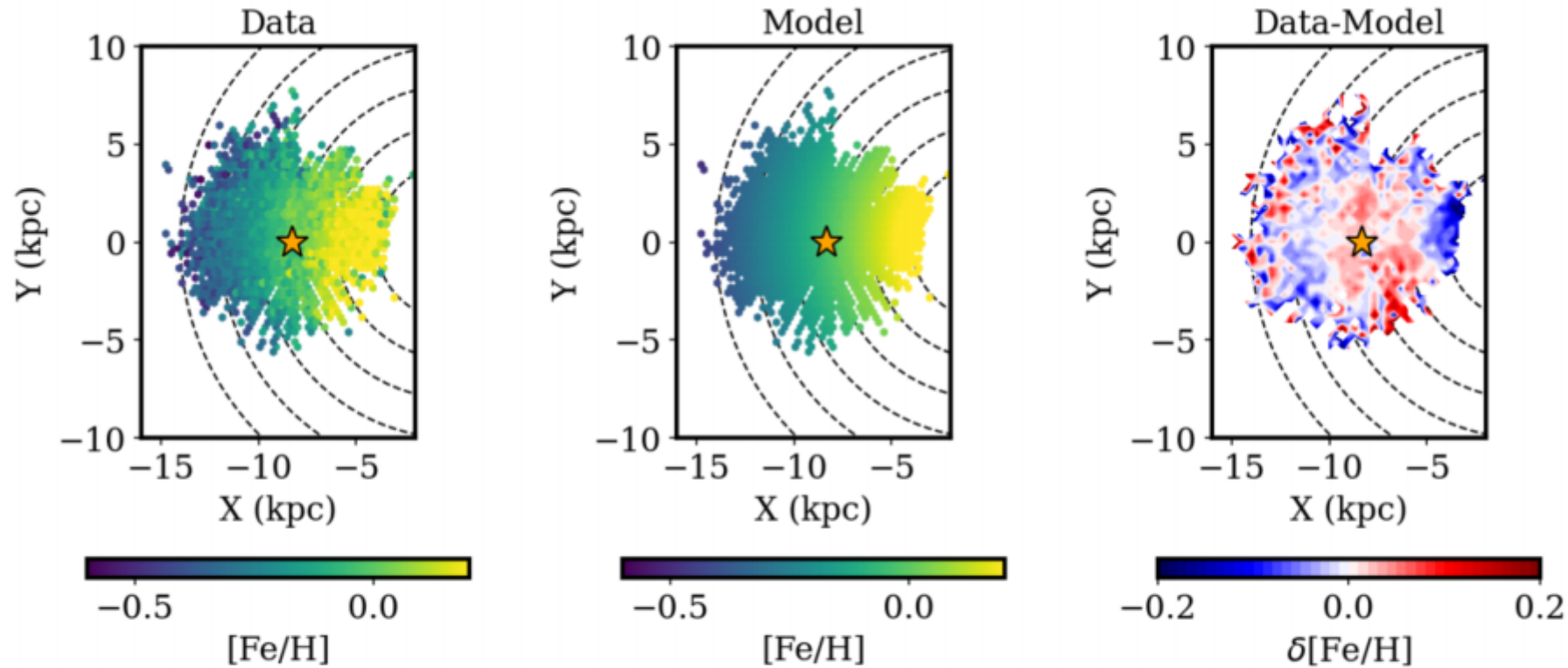


**Figure 5.** Left: The full *APOGEE* planar thin disk sample colored by the metallicity. Middle: Each position of the data points colored by a model gradient of  $\Delta[\text{Fe}/\text{H}]/\Delta R = -0.066 + 0.546 \text{ dex/kpc}$ . Right: the residuals of the observed  $[\text{Fe}/\text{H}]$  abundances and the linear model abundances.

- To probe different formation pathways for this oscillating pattern, we first compare these results with the location of the spiral arms.

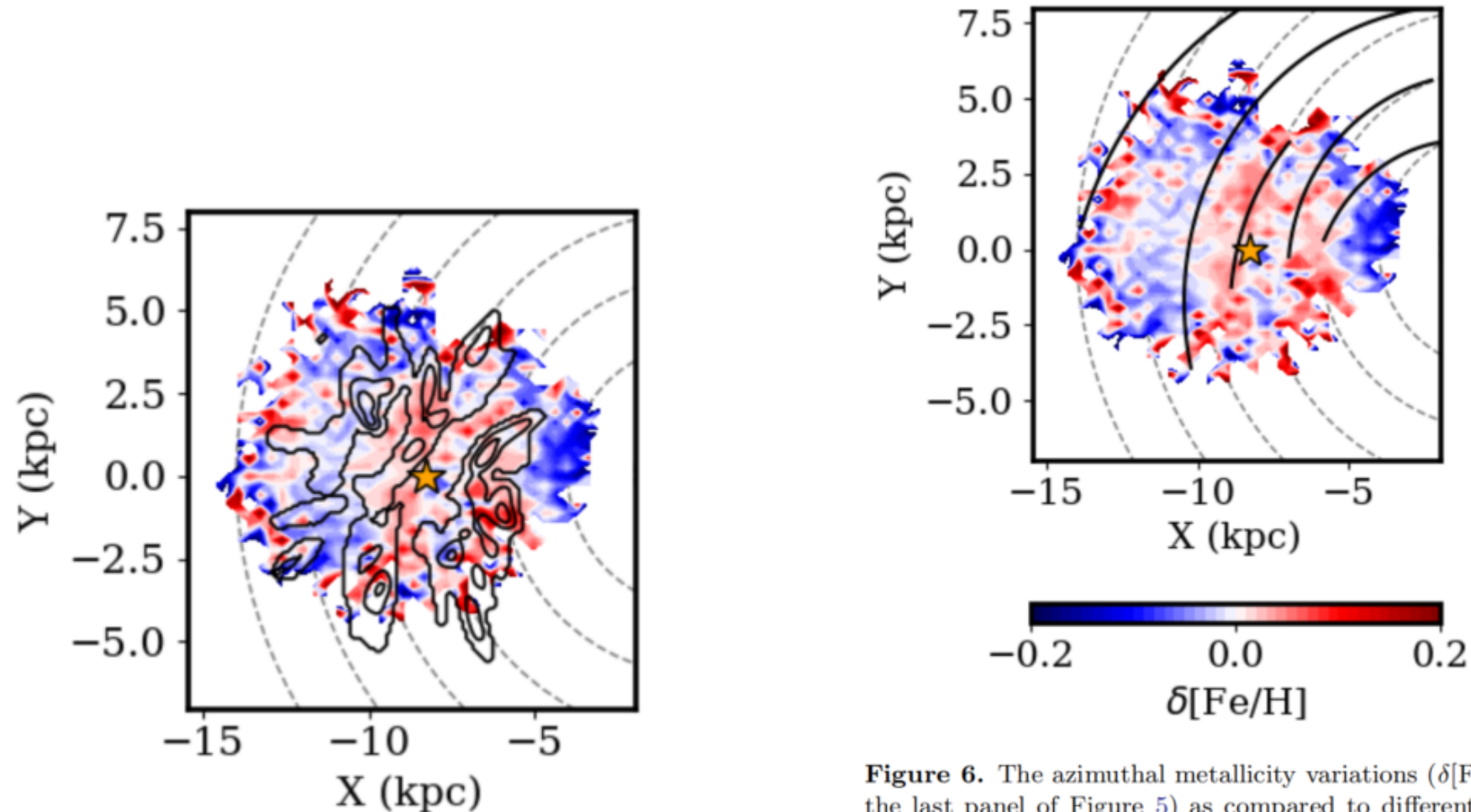


**Figure 6.** The azimuthal metallicity variations ( $\delta[\text{Fe}/\text{H}]$  in the last panel of Figure 5) as compared to different determinations of the spiral arms. The black contours in the top panel represent the spiral arms as derived by Poggio et al. (2021) using main sequence stars in *Gaia* and the solid black lines in the bottom panel are the spiral arms as determined by Reid et al. (2019) using high-mass star-forming regions.



# Azimuthal Variations in Other Elements

- Here, we explore azimuthal variations in  $[\text{Fe}/\text{H}]$  and  $\alpha$ -elements (O, Mg, Si, S, Ca) in our planar thin disk sample.

We fit linear gradients to these elements and subtracted off the linear model to look for structure in the **residuals**.

In the disk where there is a  $\delta[\text{Fe}/\text{H}]$  **excess**, there is a  $\delta[\alpha/\text{Fe}]$  **deficit**.

The anti-correlation between  $[\text{Fe}/\text{H}]$  and  $[\alpha/\text{Fe}]$  can be explained by the **astrophysical processes** (and timescales) that are largely responsible for the production of these elements.

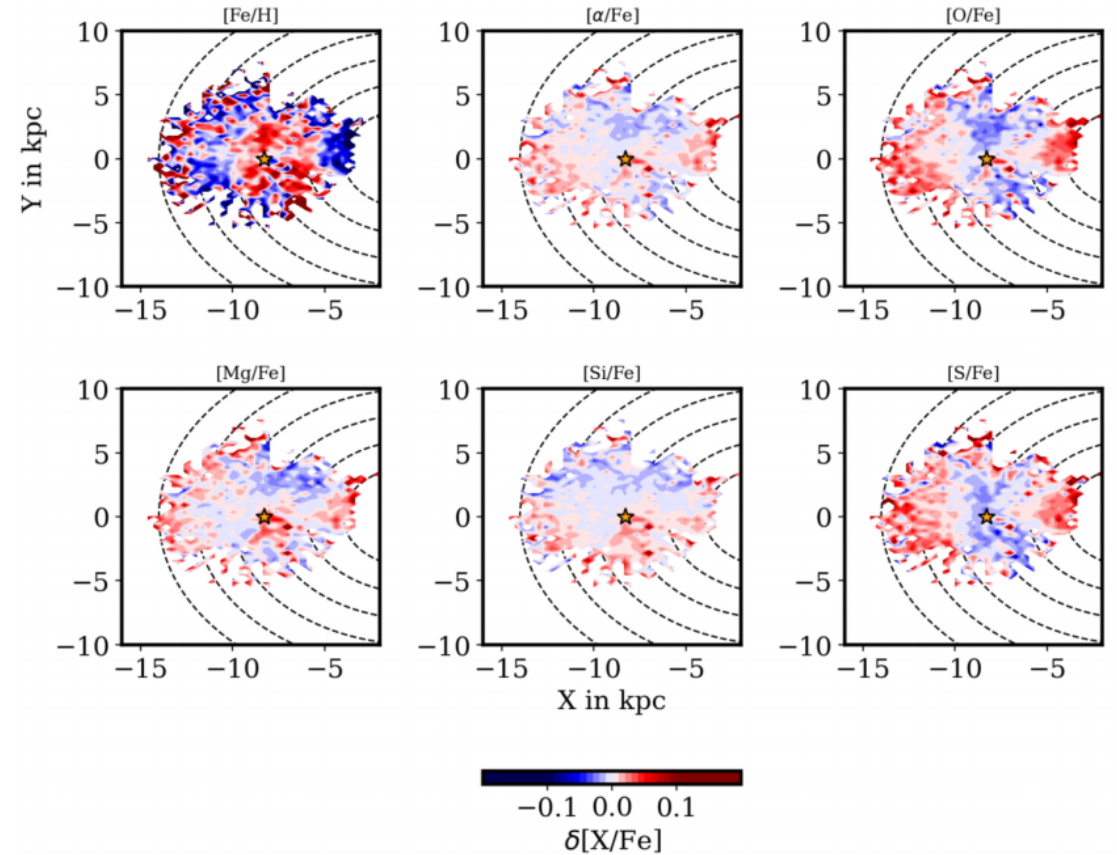


**Figure 7.** The *Data – Model* panel for the elements we deem to behave monotonically with respect to Galactocentric radius. The contours are colored by the shared  $[\text{X}/\text{Fe}]$  colorbar to illustrate the varying intensities of the deviations from the linear radial gradient. The second panel represents the average  $[\alpha/\text{Fe}]$  abundance, with the individual  $\alpha$ -elements in the following panels. The elements with the most saturated contours, such as  $[\text{Fe}/\text{H}]$ , showcase the most exaggerated deviation from the radial gradients. The  $\alpha$ -elements appear to be loosely anti-correlated with  $[\text{Fe}/\text{H}]$ , following predictions from the difference in timescales between events that mainly produce  $\alpha$ -elements (Type II SN) and events that mainly produce  $[\text{Fe}/\text{H}]$  (Type Ia SN).

# Azimuthal Metallicity Variations by Age

- Visually, the signatures seem to be the strongest in the panel containing the oldest stars, while the deviations lessen in intensity with decreasing age.

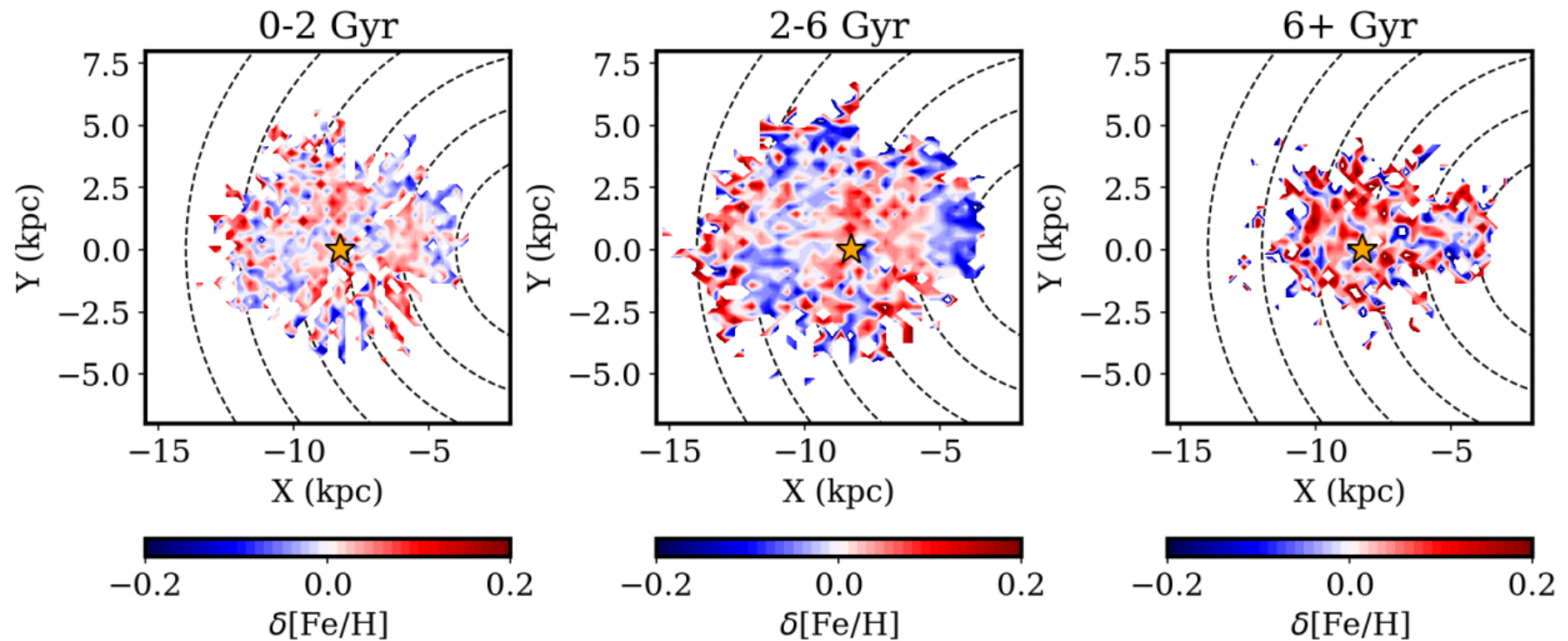


**Figure 8.** This figure is similar to Panel 3 of Figure 5 increasing age groups of 0 – 2, 3 – 6, and 6+ Gyr from left to right with 8730, 18493 and 5545 stars respectively. The color bars are constant throughout all panels, thus the youngest age group has the least amount of contrast and represents the smallest deviations from the linear gradient. Conversely, the oldest age group has the most saturated colors due to the larger variations from the modelled linear gradient.

# Azimuthal Metallicity Variations by Age

For all age groups, the variations are minimized at  $\phi(\pi) = 1$ , which is most likely due to **the sample selection** and the number of stars located along the line of sight from the Sun towards the center of the Galaxy.

The presence of the strongest azimuthal variations in our older populations suggest an important contribution from **dynamical processes** to the creation of azimuthal metallicity variations throughout the Galactic disk.

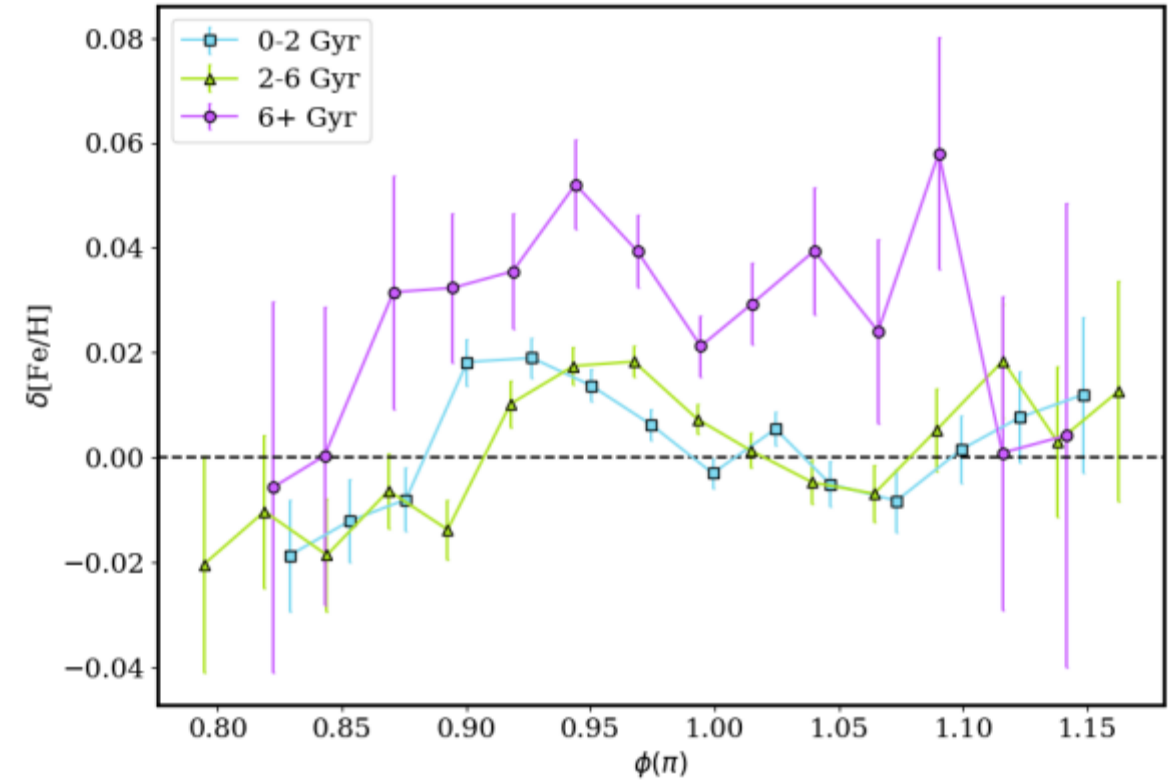


**Figure 9.** This figure shows  $\delta[\text{Fe}/\text{H}]$  as a function of azimuthal angle ( $\phi$ ). For reference,  $\phi(\pi) = 1$  is the line of sight from the Sun towards the Galactic center. The youngest age group, 0 – 2 Gyr (blue squares), displays the smallest deviations from zero in  $\delta[\text{Fe}/\text{H}]$ . The intermediate age group, 2 – 6 Gyr (green triangles), is the largest sample and has noticeable deviations from zero. The oldest age group, 6+ Gyr (purple circles), varies the most dramatically in  $\delta[\text{Fe}/\text{H}]$  azimuthally. This depiction matches the theorized azimuthal variations, discussed further in Section 4.4.

# Linking Chemistry to Dynamics

In the first and third panels of Figure 10, we see larger  $|\delta[\text{Fe}/\text{H}]|$  at higher eccentricities and radial actions. This implies that **blurring** (heating of orbits) contributes a non-negligible amount to the mechanisms that are causing these observed azimuthal metallicity variations.

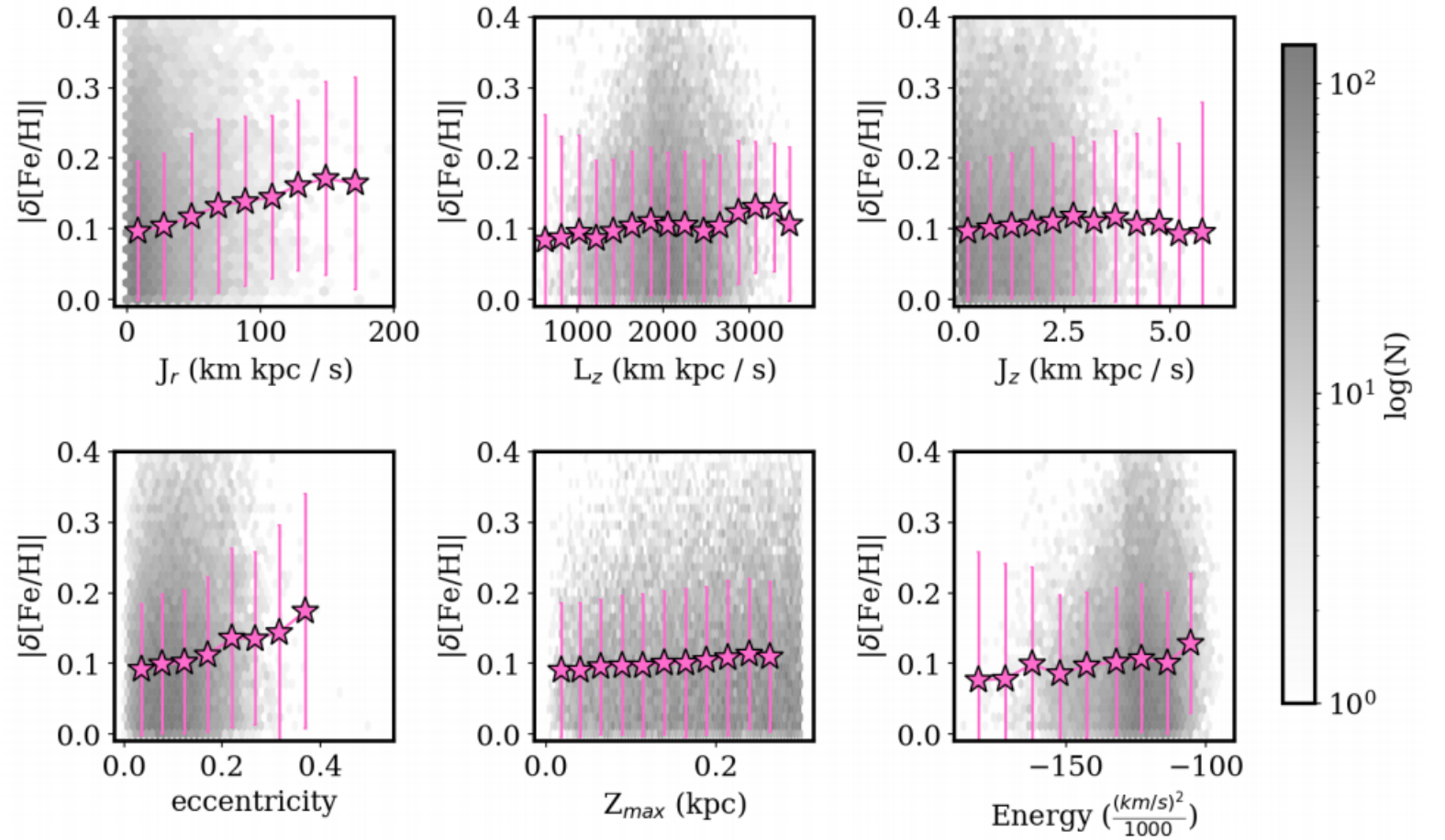


**Figure 10.** The correlation between absolute metallicity excess ( $|\delta[\text{Fe}/\text{H}]|$ ) on the y axes and different dynamical properties on the x axes. The hexagonal bins are colored by density with the pink stars representing the running medians in each panels with error bars showing the standard deviation. In the  $J_r$  and eccentricity panels, we see a clear increasing trend hinting that stars with high eccentricities and high radial actions contribute to the variations with the largest magnitudes. <sup>12</sup>



# Summary

- We aim to confirm the [Fe/H] azimuthal variations in APOGEE DR17, characterize how the variations interplay with stellar age, identify if azimuthal variations exist in elements other than [Fe/H], and attempt to link the azimuthal variations to dynamical properties.
- A radial metallicity gradient ( $\Delta[\text{Fe}/\text{H}]/\Delta R$ ) of  $\sim -0.066 \pm 0.0004 \text{ dex/kpc}$  is found throughout the kinematic thin disk of the Milky Way.
- **Azimuthal variations** are found throughout the disk in [Fe/H].
- Azimuthal substructure varies by stellar age. Older populations exhibit **more extreme deviations** from the radial metallicity gradient than seen in younger and intermediate populations.



# Summary

- There is **a positive trend** between  $|\delta[\text{Fe}/\text{H}]|$  and  $J_r$ , as well as  $|\delta[\text{Fe}/\text{H}]|$  and eccentricity. Hinting that **blurring** is an important dynamical process in the production of azimuthal  $[\text{Fe}/\text{H}]$  variations.